Two Functionally Distinct 4-Aminopyridine-sensitive Outward K^+ Currents in Rat Atrial Myocytes

WALTER A. BOYLE and JEANNE M. NERBONNE

From the Departments of Molecular Biology & Pharmacology and Anesthesiology, Washington University School of Medicine, St. Louis, Missouri 63110

ABSTRACT In the experiments here, the detailed kinetic properties of the Ca^{2+}-independent, depolarization-activated outward currents (I_{out}) in enzymatically dispersed adult rat atrial myocytes were studied. Although there is only slight attenuation of peak I_{out} during brief (100 ms) voltage steps, substantial decay is evident during long (10 s) depolarizations. The analyses here reveal that current inactivation is best described by the sum of two exponential components, which we have termed I_{Kf} and I_{Ks} to denote the fast and slow components, respectively, of I_{out} decay. At all test potentials, I_{Kf} inactivates ~20-fold more rapidly than I_{Ks}. Neither the decay time constants nor the fraction of I_{out} remaining at the end of 10-s depolarizations varies over the potential range of 0 to +50 mV, indicating that the rates of inactivation and recovery from inactivation are voltage independent. I_{Kf} recovers from inactivation completely, independent of the recovery of I_{Ks}, and I_{Kf} recovers ~20 times faster than I_{Ks}. The pharmacological properties of I_{Kf} and I_{Ks} are similar: both components are sensitive to 4-aminopyridine (1–5 mM) and both are relatively resistant to externally applied tetraethylammonium (50 mM). Taken together, these findings suggest that I_{Kf} and I_{Ks} correspond to two functionally distinct K^+ currents with similar voltage-dependent properties and pharmacologic sensitivities, but with markedly different rates of inactivation and recovery from inactivation. From the experimental data, several gating models were developed in which voltage-independent inactivation is coupled either to channel opening or to the activation of the individual channel subunits. Experimental testing of predictions of these models suggests that voltage-independent inactivation is coupled to activation, and that inactivation of only a single subunit is required to result in functional inactivation of the channels. This model closely approximates the properties of I_{Kf} and I_{Ks}, as well as the composite outward currents, measured in adult rat atrial myocytes.

Address reprint requests to Dr. Jeanne M. Nerbonne, Department of Molecular Biology & Pharmacology, Washington University Medical School, 660 South Euclid Avenue, St. Louis, MO 63110.

J. GEN. PHYSIOL. © The Rockefeller University Press · 0022-1295/92/12/1041/27 $2.00
Volume 100 December 1992 1041–1067

INTRODUCTION

In the mammalian myocardium, various types of depolarization-activated outward K^+ currents have been distinguished based on differences in time- and voltage-dependent properties and pharmacological sensitivities (Cohen, Datyner, Gintant, and Kline, 1986; Carmeliet, Biermans, Callawaert, and Vereecke, 1987). Transient outward currents, for example, are characterized by rapid activation and inactivation kinetics and sensitivity to millimolar concentrations of 4-aminopyridine (4-AP) (Kenyon and Gibbons, 1979; Coraboeuf and Carmeliet, 1982; Kukushkin, Gainullin, and Sosunov, 1983; Giles and Van Ginneken, 1985; Nakayama and Irisawa, 1985; Escande, Coulombe, Faivre, Deroubaix, and Corabouef, 1987; Kenyon and Sutko, 1987; Tseng, Robinson, and Hoffman, 1987; Benndorf and Nilius, 1988; Giles and Imaizumi, 1988; Apkon and Nerbonne, 1991). In Purkinje fibers and some cardiac myocytes, Ca^{2+}-dependent transient outward currents have also been described; these currents are blocked selectively by agents that inhibit voltage-dependent Ca^{2+} influx or intracellular Ca^{2+} release, and they are 4-AP resistant (Coraboeuf and Carmeliet, 1982; Escande et al., 1987; Kenyon and Sutko, 1987; Tseng et al., 1987; Giles and Imaizumi, 1988). Delayed outward K^+ currents in mammalian cardiac preparations, although somewhat less well characterized, have been distinguished (from transient currents) by slower activation and inactivation kinetics (McDonald and Trautwein, 1978; Hume and Uehara, 1985; Tseng et al., 1987; Giles and Imaizumi, 1988) and greater sensitivity to extracellular tetraethylammonium (Apkon and Nerbonne, 1991).

Recently, we reported the presence of a novel type of Ca^{2+}-independent, depolarization-activated outward K^+ current (I_{out}) in adult rat atrial myocytes with properties distinct from those of either the transient or delayed K^+ currents described in other cardiac preparations (Boyle and Nerbonne, 1991). Although I_{out} in these cells activates rapidly and is blocked by 4-AP, it is distinct from other myocardial transient K^+ currents in that peak I_{out} decays only slightly (15.7 ± 10.0%; mean ± SD) during brief (100 ms) depolarizations. The time- and voltage-dependent properties and the pharmacological sensitivity of atrial I_{out} are also distinct from those of delayed outward K^+ currents described in other cardiac preparations. Interestingly, the properties of the atrial currents closely resemble those of several K^+ channels cloned from rat brain and, more recently, rat heart, cDNA libraries, and expressed in *Xenopus* oocytes (Stühmer, Stocker, Sakmann, Seeburg, Baumann, Grupe, and Pongs, 1988; Christie, Adelman, Douglass, and North, 1989; Stühmer, Ruppersberg, Schröter, Sakmann, Stocker, Giese, Baumann, and Pongs, 1989; Grupe, Schröter, Ruppersberg, Stocker, Drewes, Beckh, and Pongs, 1990; Koren, Liman, Logothetis, Nadal-Ginard, and Hess, 1990; Swanson, Marshall, Smith, Williams, Boyle, Folander, Luneau, Antanavage, Oliva, Buhrow, Bennett, Stein, and Kaczmarek, 1990; Tseng-Crank, Tseng, Schwartz, and Tanouye, 1990; Paulmichl, Nasmith, Hellmiss, Reed, Boyle, Nerbonne, Peralta, and Clapham, 1991; Roberds and Tamkun, 1991).

Although there is little attenuation of peak atrial I_{out} during brief depolarizations, substantial decay is evident during prolonged (10 s) depolarizations. Inactivation of atrial I_{out} is best described by the sum of two exponential components, which we have termed I_{Kf} and I_{Ks} to denote the fast and the slow components, respectively, of I_{out}

decay. The analyses here also reveal that I_{Kf} and I_{Ks} recover from inactivation independently and over substantially different time courses, indicating that I_{Kf} and I_{Ks} reflect currents through two functionally distinct populations of depolarization-activated K^+ channels. The other time- and voltage-dependent properties and the pharmacological sensitivities of I_{Kf} and I_{Ks}, however, are indistinguishable. Several gating models were developed from the experimental data which were capable of generating currents with time- and voltage-dependent properties similar to those of I_{Kf} and I_{Ks}, as well as those of the composite whole-cell current, I_{out}. Predictions of these models were then tested experimentally, and one was found to approximate very closely all of the properties of the depolarization-activated K^+ currents in adult rat atrial myocytes.

METHODS

Preparation of Isolated Myocytes

Single atrial myocytes were isolated from adult rat heart using a procedure developed in this laboratory from procedures described previously by others (Powell and Twist, 1976; Wittenberg and Robinson, 1981). In brief, hearts were rapidly removed from anesthetized (halothane/O_2) adult Long Evans rats (200–250 g) and retrogradely perfused (at 37°C) through the aorta with Ca^{2+}-free Krebs buffer (50 ml) followed by perfusion with buffer containing either 0.10–0.2% type II collagenase (Worthington Biochemical Corp., Freehold, NJ) or 0.01–0.02% type IA collagenase (Sigma Chemical Co., St. Louis, MO) and 10 μM added Ca^{2+}. During perfusion, the hearts were kept immersed in the Krebs-enzyme solution, which was filtered (5 μm) and recirculated until the hearts were digested (20–40 min). After perfusion, the atrial appendages were removed, cut into small pieces, incubated in fresh Krebs-enzyme buffer for an additional 5–20 min, and mechanically dispersed with a fire-polished Pasteur pipette. The tissue was then filtered through gauze to remove undigested fragments and washed twice in enzyme-free Krebs containing 150 μM Ca^{2+}. The filtrate was enriched for rod-shaped cells by low speed centrifugation (300–500 rpm; 10 min). Dissociated cells were resuspended in serum-free Medium-199 (Irvine Scientific, Santa Ana, CA) supplemented with antibiotics (penicillin/streptomycin) and plated on glass coverslips coated with laminin (Collaborative Research, Inc., Bedford, MA). Rod-shaped, Ca^{2+}-tolerant myocytes adhered preferentially to the laminin substrate and damaged, rounded-up cells were removed by replacing the medium 5–10 min and again 30–60 min after plating.

Dissociated myocytes were maintained at 37°C in a humidified air/CO_2 (95:5) environment and many myocytes remained rod-shaped for 24–96 h in vitro. Because we wished to study a homogeneous population of cells, all experiments were performed on rod-shaped atrial myocytes within 48 h of isolation.

Electrophysiological Recordings

The whole-cell variation of the patch-clamp technique (Hamill, Marty, Neher, Sakmann, and Sigworth, 1981) was used to record depolarization-activated K^+ currents in isolated adult rat atrial myocytes. All recordings were performed at room temperature (21–23°C). The voltage-clamp circuit was provided by an Axopatch-1B (0.5 GΩ feedback resistor; Axon Instruments, Inc., Foster City, CA) whole-cell/patch-clamp amplifier. Recording pipettes were fabricated from borosilicate glass, coated with Sylgard (Dow Corning Corp., Midland, MI), and fire-polished to produce electrodes with tip diameters of 1.0–2.0 μm and resistances of 2–4 MΩ when filled with recording solution (see below). After formation of a high resistance giga seal

(range 2–10 GΩ), electrode capacitance was compensated before obtaining the whole-cell configuration.

In the whole-cell configuration, series resistances, estimated from the decay of the uncompensated capacitative transients, were found to equal 1.5–2 times the pipette resistance. Because series resistance was routinely compensated by >80% and peak outward current amplitudes were generally <5 nA, voltage errors due to uncompensated series resistance were small (≤8 mV) and were not corrected. In all experiments, series resistance was checked at regular intervals to ensure that no variations occurred over time; if measurable increases developed, the experiment was discontinued and the data were not subsequently analyzed. Only cells with input resistances ≥0.4 GΩ were studied (range: 0.4–1.5 GΩ).

To measure Ca^{2+}-independent, depolarization-activated outward K^+ currents, bath solutions routinely contained (mM): 136 NaCl, 4 KCl, 1 $CaCl_2$, 2 $MgCl_2$, 10 HEPES, 10 glucose, 5 $CoCl_2$, and 0.02 tetrodotoxin (TTX) at pH 7.2–7.4, 300–310 mosmol. In some experiments, designed to explore the effects of high extracellular divalent cation concentrations and Co^{2+} on the properties of the atrial K^+ currents, the Co^{2+} was replaced by 1 mM Cd^{2+} and 1 μM nifedipine was added to ensure the complete block of voltage-gated Ca^{2+} currents. These experiments (n = 8) revealed that the measured properties of the currents in these cells were largely unaffected, although there was a small shift (−3 mV) in the $V_{1/2}$ for current activation as compared with the currents recorded in the presence of 5 mM Co^{2+}. All of the current waveforms displayed and analyzed here were obtained under the routine recording conditions, i.e., with 5 mM Co^{2+} in the bath. Although the bath solution contained 20 μM TTX, complete block of voltage-dependent Na^+ currents (I_{Na}) was not always provided due to the presence of a TTX-resistant component of I_{Na} in these cells (Reuter, 1984). In addition, the amplitude of the TTX-resistant component of I_{Na} varied considerably among cells.

Recording pipettes routinely contained (mM): 135 KCl, 10 EGTA, 10 HEPES, 5 glucose with 3 Mg-ATP, and 0.5 Tris-GTP (pH 7.2, 300–310 mosmol). To determine if this high intracellular Cl^- concentration influenced the measured properties of these cells in general, or the outward K^+ currents in particular, experiments were also completed using K-aspartate in place of the KCl in the recording pipettes. These experiments (n = 6) revealed that there are no measurable effects on the time- or voltage-dependent properties of the measured K^+ currents in these cells as a function of the concentration of Cl^- or aspartate$^-$ in the recording pipettes. All of the current waveforms displayed and analyzed here were obtained under the routine recording conditions, i.e., with 135 mM KCl in the recording pipettes.

Outward K^+ currents were routinely measured during depolarizations to membrane potentials between −40 and +50 mV from a holding potential (HP) of −60 mV. This HP was chosen to minimize contamination of the outward current waveforms by the TTX-resistant component of I_{Na} (see above). For studies of voltage-dependent inactivation, however, the range of HPs was −110–0 mV. Experimental parameters such as HPs, test potentials, and the timing of voltage steps were controlled with an AST-286 or Northgate 386 equipped with a Tecmar Labmaster (Scientific Solutions Inc., Solon, OH) analog/digital interface. Data acquisition was performed using pCLAMP (v4.1; Axon Instruments Inc.). Sampling frequencies ranged from 4 to 10 kHz and current signals were filtered at 3–5 kHz (corner frequency) before digitization and storage. All of the current records displayed (and all of the currents analyzed here) are raw records and no corrections have been made for linear "leakage" currents which are negligible in cells with input resistances of ≥0.4 GΩ. On average, atrial cells are 15 × 100 μm, yielding an estimated surface area of 5×10^{-5} cm^2, assuming the cells are cylindrical (Boyle and Nerbonne, 1991). Integration of the capacitative transients evoked during small voltage steps from a HP of −70 mV provided a mean (±SD) membrane capacitance of 58.0 ± 16.5 pF (n = 13) for these cells.

4-AP (Sigma Chemical Co.) and tetraethylammonium (TEA; Sigma Chemical Co.) were applied to isolated myocytes during electrophysiological recordings by pressure ejection from

small (2–3 μm) puffer pipettes placed within ~20 μm of the cell surface. At least two puffer pipettes were used; one contained only bath solution and served as a control. 4-AP was dissolved in bath solution immediately before use. The TEA-containing solution was prepared by equimolar substitution (50 mM) of TEACl (Sigma Chemical Co.) for NaCl in the standard bath solution.

Data Analyses

Data were compiled and analyzed using pCLAMP, Lotus 1-2-3 (Lotus Corporation, Cambridge, MA), and NFIT (Island Products, Galveston, TX). The kinetics of outward current decay were analyzed using Clampfit (pCLAMP) as described in the text and the time constants and magnitudes of the current components were determined from the fitting procedure. In several cases, the experimental data and the results provided by the current simulations (see below) were analyzed using NFIT with functions presented in the text. Additional components were included in the fitting equations only if they substantially improved the quality of the fits as judged by the correlation coefficient (R) and by eye. Examples of fits are displayed in the figures together with the data points. All averaged and normalized data are presented as mean ± either the standard deviation of the mean (±SD) or the standard error of the mean (±SEM), as indicated. Statistical significance was examined using the analysis of variance (ANOVA).

Model Simulations

For modeling the atrial outward currents, a diagram was constructed of the kinetic states of the channels, and differential equations were written describing the time-dependent changes in the probability of channels existing in each of the proposed states. Simulations were accomplished using TUTSIM (Tutsim Products, Palo Alto, CA), with the instantaneous probabilities over time obtained by numerical integration at an interval of 100 μs. The modeled currents were generated at the same rate by multiplying the open state probability by the driving force, $V_m - V_{rev}$, where V_m is the membrane potential and V_{rev} is the mean measured reversal potential of −75.5 mV (Boyle and Nerbonne, 1991) of the currents (see text). Voltage-dependent activation (α) and deactivation (β) rate constants were derived from the analyses of the voltage dependences and activation rates of the measured currents (see text). Voltage-independent inactivation (κ) and recovery (λ) rate constants were derived from the inactivation and recovery data. In testing the models, the absolute values of κ and λ were adjusted until the inactivation and recovery kinetics of the simulated currents, as well as the amount of the noninactivating current, closely resembled those observed in the electrophysiological experiments.

RESULTS

Time- and Voltage-dependent Activation and Inactivation

Representative Ca^{2+}-independent depolarization-activated outward K^+ current (I_{out}) waveforms evoked in an isolated adult rat atrial myocyte during depolarizations to potentials between −40 and +50 mV from a HP of −60 mV are displayed in Fig. 1. All of the experiments here were completed with inward Ca^{2+} current blocked by the Co^{2+} in the bath. To date, we have not explored the effects of changing the intracellular or extracellular Ca^{2+} concentration on the measured properties of these currents, and we have not determined if there are any Ca^{2+}-dependent K^+ currents in these cells. As previously reported (Boyle and Nerbonne, 1991), on membrane depolarization, I_{out} activates rapidly after a delay and the time course of activation is well described by a fourth power exponential. In addition, current amplitudes as well

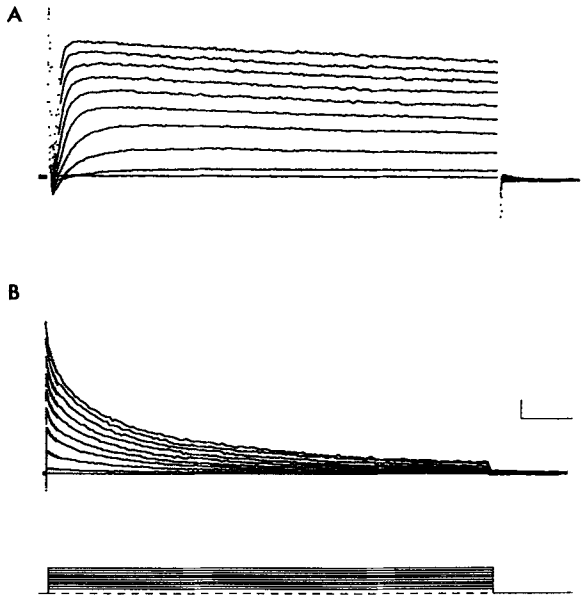

FIGURE 1. Activation and inactivation of depolarization-activated outward K^+ currents (I_{out}) in an isolated adult rat atrial myocyte. Depolarizations from a HP of −60 mV to potentials between −40 and +50 mV were applied in 10-mV increments. Co^{2+} (5 mM) and TTX (20 μM) were present in the bath to block voltage-gated inward Ca^{2+} and Na^+ currents, respectively. (*A*) 100-ms steps presented at 5-s intervals. Current amplitudes and activation rates increase with increasing depolarization and there is little or no attenuation of peak I_{out} during the steps. The largest and most rapidly activating current was evoked at +50 mV. (*B*) 10-s steps presented at 60-s intervals in the same cell. Substantial inactivation of peak I_{out} develops over several seconds. Calibration bars: 1 nA and 10 ms (*A*); 1 nA and 900 ms (*B*).

as activation rates increase with increasing depolarization (Fig. 1 *A*). Although during brief (100 ms) depolarizations (Fig. 1 *A*) I_{out} decays only slightly, substantial inactivation of peak I_{out} develops over several seconds (Fig. 1 *B*).

As illustrated in Fig. 2 *A*, decay of I_{out} during 10-s depolarizations is well described

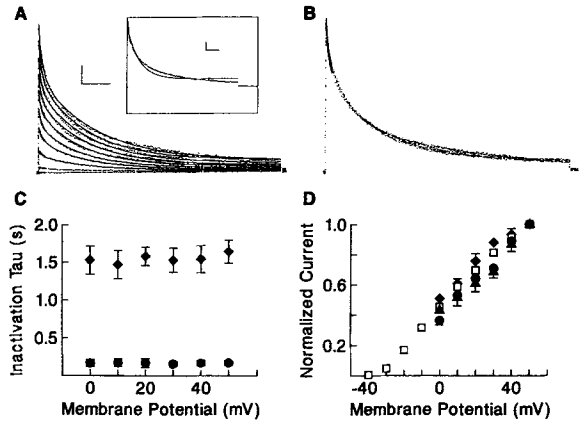

FIGURE 2. Kinetics of outward current inactivation. (*A*) The outward currents displayed in Fig. 1 *B* are replotted here (as points) with double exponential fits (*solid lines*) to the decay phases of the currents superimposed. (*Inset*) Single exponential fit to the decay phase of the current evoked at +50 mV. (*B*) I_{out} waveforms recorded at test potentials between 0 and +50 mV (from *A*) are superimposed after each was scaled to the peak I_{out} recorded at +50 mV. (*C*) Mean (±SEM; n = 5) values for the fast (●) and slow (◆) inactivation time constants plotted as a function of test potential. (*D*) Mean (± SEM; n = 5) normalized current–voltage relations for peak I_{out} (□), I_{Kf} (●), I_{Ks} (◆), and I_{ss} (▲); all of the currents were normalized to their respective values at +50 mV. Calibration bars: 1 nA and 900 ms (*A*, *B*).

by a double exponential function of the form:

$$I_{out}(t) = I_{Kf} * [\exp(-t/\tau_f)] + I_{Ks} * [\exp(-t/\tau_s)] + I_{ss} \quad (1)$$

where I_{Kf} and I_{Ks} are the rapidly and slowly inactivating fractions of the total outward current; τ_f and τ_s are the inactivation time constants of the rapidly and slowly decaying components; and I_{ss} is the steady-state current (see also below for further clarification of these terms). The fits were not as good when a single exponential was used (see Fig. 2 *A*, *inset*).

The values for τ_f and τ_s display no measurable voltage dependence over the potential range of 0 to +50 mV (Fig. 2 *C*). In addition, the magnitudes of I_{Kf}, I_{Ks}, and I_{ss} increase in parallel with that of peak I_{out} over this same potential range. This is demonstrated by scaling and superimposing the currents recorded at various potentials in individual cells (Fig. 2 *B*), or by analysis of the normalized current–voltage relations for peak I_{out}, I_{Kf}, I_{Ks}, and I_{ss} in several cells (Fig. 2 *D*). These results suggest that the voltage dependences of activation of I_{Kf} and I_{Ks} are indistinguishable (see also below). In addition, assuming that I_{ss} reflects incomplete inactivation of I_{out} (i.e., incomplete inactivation of I_{Kf} and I_{Ks}), these results suggest that the rate constants

TABLE I

Components of Atrial I_{out}

	Inactivation τ		Current fraction (I/I_{out})	
	Mean (±SD)	Range	Mean (±SD)	Range
	ms			
I_{Kf}	181 ± 124	62–480	0.32 ± 0.14	0–0.50
I_{Ks}	3,006 ± 1,016	1,157–5,837	0.47 ± 0.16	0.17–0.89
I_{ss}	—	—	0.21 ± 0.10	0.09–0.44

governing inactivation and recovery from inactivation of I_{Kf} and I_{Ks} are voltage independent. It should be noted that the assumption that I_{ss} represents the noninactivating fractions of I_{Kf} and I_{Ks} is made throughout the remainder of this paper. Although difficult to prove experimentally, this assumption is consistent with all of the experimental data (as discussed below). Thus, although the terms I_{Kf} and I_{Ks} in Eq. 1 (above) and elsewhere in the text refer to the amplitudes of the inactivating fractions of the currents, the actual amplitudes of the two current components include the noninactivating fraction of each, represented by I_{ss}.

Because the values for τ_f and τ_s, as well as the relative magnitudes of I_{Kf} and I_{Ks}, are unaffected by voltage over the potential range 0 to +50 mV, long depolarizations to a single test potential of +50 mV were presented to characterize I_{out} inactivation in 38 additional atrial cells (Table I). In all but 2 of these 38 cells, two exponentials were required to describe the time course of I_{out} decay, and in all cells examined there was an I_{ss} component, i.e., an outward current remaining at the end of the 10-s test pulses. There was some cell to cell variability in the values of τ_f and τ_s (Table I), although in most cells the ratio of τ_s to τ_f was ≥ 10, with a mean (±SD) value for τ_s/τ_f of 23.0 ± 13.6 (n = 36). Variability in the relative contribution of the two current

components to the peak I_{out} was also evident, although generally I_{Ks} was larger than I_{Kf} (Table I). As would be expected, the relatively small amount of inactivation of peak I_{out} observed during brief (100 ms) depolarizations of 15.7 ± 10% (mean ± SD) correlates with the amount of I_{Kf} inactivation predicted by the fits of peak I_{out} decay during long depolarizations (R = 0.95). Thus, the variability in peak I_{out} inactivation during brief depolarizations (Boyle and Nerbonne, 1991) appears to result from cell to cell variability in the relative contribution of I_{Kf} to the peak I_{out}, as well as the precise value of τ_f.

Recovery from Inactivation

The time courses of recovery from inactivation of peak I_{out}, I_{Kf}, and I_{Ks} were examined in paired pulse experiments in which two successive 10-s depolarizing pulses to +50 mV from a HP of −60 mV were applied at interpulse intervals ranging from 10 ms to 60 s. The decay phase of I_{out} evoked during the first pulse was fitted according to Eq. 1 and the time constants derived from that fit were then used to fit I_{out} decay during the second pulse of the pair. For each pair of pulses, the magnitudes of peak I_{out}, I_{Kf}, and I_{Ks} derived from the fits were compared to determine the amount of recovery for a given interpulse interval; the cell was held at −60 mV for 60 s between pulse pairs to allow complete recovery of peak I_{out}. A sequence of four paired pulses (to the same cell) in which the interpulse interval was varied from 3 to 52 s is shown in Fig. 3. The data and the fits for each pulse pair are displayed, and the magnitudes and percent changes in peak I_{out}, I_{Kf}, and I_{Ks} are given in the insets of the figure. Although the various parameters (e.g., I_{Kf}, τ_f, etc.) were left free when each of the control current waveforms was fitted, there were no significant differences in the values obtained from these fits (see insets) even though the time required to complete these experiments was rather long and the total time between recording the control currents for each paired pulse experiment was several minutes. These data demonstrate that the properties of the currents do not vary substantially over time.

For the cell in Fig. 3, peak I_{out} recovered to ~80% of the control value and I_{Kf} recovered completely when the interpulse interval was 3 s (Fig. 3 *A*). The remaining ~20% of the peak I_{out} recovered over a much longer time course, and complete recovery was only evident when the interpulse interval was increased to 52 s (Fig. 3, *B–D*). The slow phase of peak I_{out} recovery was due to the slow recovery of I_{Ks} (Fig. 3, *insets*). Thus, I_{Kf} recovers from steady-state inactivation completely independent of the recovery of I_{Ks}.

Paired pulse experiments, such as that illustrated in Fig. 3, required long periods of stable recording conditions. As such, increased series resistances or "leak" currents often resulted in premature termination of these experiments before sufficient data over a wide range of interpulse intervals could be collected. Nevertheless, in a total of 20 atrial cells, long enough interpulse intervals were tested to demonstrate the complete recovery of I_{Kf} "independent" of the recovery of I_{Ks} (similar to the results presented in Fig. 3). Although the complete recovery of I_{Ks} (and peak I_{out}) was not demonstrated in all of these cells, sufficient data were obtained over a range of interpulse intervals in six cells to demonstrate the complete recovery of both I_{Kf} and I_{Ks} (Fig. 4). In all six of these cells, the complete recovery of I_{Kf} (Fig. 4 *A*) occurred independent of the complete recovery of I_{Ks} (Fig. 4 *B*). These experiments confirmed

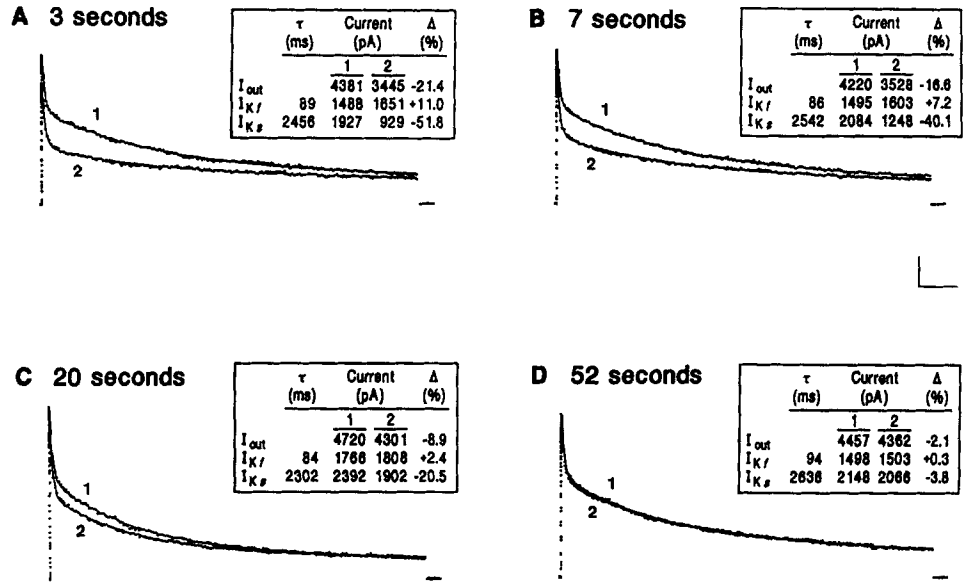

FIGURE 3. Recovery of I_{out} from inactivation. Pairs of 10-s depolarizing pulses to +50 mV from a HP of −60 mV were applied at interpulse intervals of (*A*) 3 s, (*B*) 7 s, (*C*) 20 s, and (*D*) 52 s; 60 s was allowed between each pair of pulses to allow complete recovery of peak I_{out}. The decay phases of the currents (plotted as points) were fitted (*solid lines*) with double exponential functions. In each case, the fast and slow time constants determined from the fit of the current recorded during the first pulse of each pair (*1*) was used to fit the second current waveform (*2*) recorded. (*Insets*) The amplitudes of peak I_{out}, I_{Kf}, and I_{Ks} derived from the fits for the first (*1*) and second (*2*) records of each pulse pair are listed. The percent change (Δ) in each component was calculated as = $[(I_2 - I_1)/I_1] * 100$. Calibration bars: 800 pA and 1 s (*A–D*).

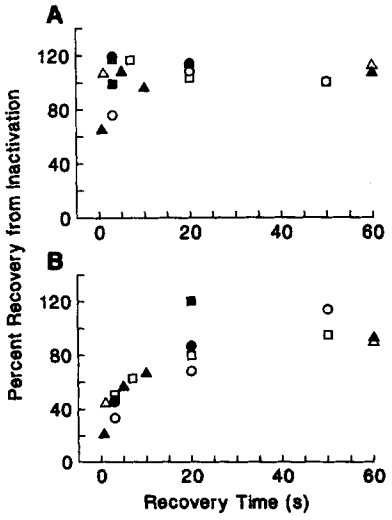

FIGURE 4. Time course of recovery from inactivation of (*A*) I_{Kf} and (*B*) I_{Ks} during paired pulse experiments similar to those illustrated in Fig. 3. The time courses of recovery of I_{Kf} and I_{Ks} were determined from double exponential fits to the decay phases of I_{out} recorded during pairs of 10-s depolarizing pulses to +50 mV (as in Fig. 3). Data obtained from six atrial cells are presented; each cell is indicated by a different symbol. (*A*) In general, I_{Kf} recovered rapidly and completely after interpulse intervals that left I_{Ks} substantially inactivated, e.g., at times ≤ 10 s. (*B*) In all six cells, however, I_{Ks} recovered (to $\geq 90\%$ of control) after long interpulse intervals.

that the long interpulse intervals required for complete recovery of peak I_{out} were clearly the result of the slow recovery of I_{Ks}. In addition, comparison of the time course of recovery suggests that I_{Kf} recovers from steady-state inactivation ~20 times faster than I_{Ks}.

The finding that I_{Kf} recovers from inactivation independent of the recovery of I_{Ks} is most simply interpreted as suggesting that I_{Kf} and I_{Ks} are functionally independent currents. This concept can be viewed intuitively by considering that the complete recovery of I_{Kf} from inactivation requires the recovery of all of the I_{Kf} channels that opened during the depolarization. This, in turn, implies full recovery of the channels in each and every kinetic state connected to the open and/or inactivated state(s) of I_{Kf} channels. Thus, if I_{Kf} and I_{Ks} share kinetic states such that some channels initially inactivating via the I_{Kf} pathway end up in the I_{Ks} pathway, the net effect will be that any I_{Ks} channels that remain inactivated would decrease the number of channels available to open via I_{Kf} in a subsequent depolarization, thereby reducing the magnitude of the I_{Kf} relaxation. In other words, the complete recovery of I_{Kf} would depend on the recovery of I_{Ks}. Therefore, because I_{Kf} recovers fully while I_{Ks} remains substantially inactivated, I_{Kf} and I_{Ks} cannot share any kinetic states. I_{Kf} and I_{Ks} must, therefore, be *functionally* independent currents.

To test this hypothesis directly and to examine the molecular mechanisms underlying the gating of these channels, we constructed models of channel gating incorporating the general features of voltage-dependent activation through multiple closed states and voltage-independent inactivation. The models used were similar to those proposed by others (Clark, Giles, and Imaizumi, 1988; Koren et al., 1990; Zagotta and Aldrich, 1990).

Gating Models of Atrial I_{out}

As noted above, we interpreted the finding that I_{Kf} and I_{Ks} recover from inactivation independently as suggesting that these two current components reflect the presence of functionally distinct K^+ channels or gating pathways. To test this hypothesis directly, we began the modeling by considering gating models incorporating two inactivated states of the same channel, which could be populated either sequentially or in parallel from the open state, to account for the two inactivation and recovery time constants for peak atrial I_{out}.

Models of atrial I_{out} were based on the kinetic and voltage-dependent properties of the measured currents. Because the kinetics of I_{out} activation appeared not to be dependent on the relative amplitudes of I_{Kf} and I_{Ks}, we assumed in this initial modeling that the time and voltage dependences of I_{Kf} and I_{Ks} activation were the same (see below). For simplicity, we also assumed that both components had the same reversal potential (of approximately −75 mV) of the peak I_{out} reported previously (Boyle and Nerbonne, 1991; see also below). Atrial I_{out} activates with a delay and the time course of activation is best described by a fourth power exponential of the form: $I_{out}(t) = I_{max}\,[1\text{-}\exp(-t/\tau_n)]^4$ (Fig. 5 *A*). Therefore, the Hodgkin and Huxley (1952) n^4 model was used in which channel opening requires activation of four independent subunits (or gating particles) governed by voltage-dependent forward (α) and reverse (β) activation rate constants. This results in four closed states (C) which must be traversed before opening (O) according to the

following kinetic scheme:

$$C_1 \underset{\beta}{\overset{4\alpha}{\rightleftharpoons}} C_2 \underset{2\beta}{\overset{3\alpha}{\rightleftharpoons}} C_3 \underset{3\beta}{\overset{2\alpha}{\rightleftharpoons}} C_4 \underset{4\beta}{\overset{\alpha}{\rightleftharpoons}} O \qquad \text{(A)}$$

Values for α and β were calculated from the activation time constants (τ_n) and the voltage-dependent steady-state probabilities of activation (n_∞) of each subunit, where $\alpha = n_\infty/\tau_n$ and $\beta = (1 - n_\infty)/\tau_n$. Values for τ_n at each voltage were determined from the activation time course of I_{out} described above (Fig. 5 *A*) and values for n_∞ were extracted from the normalized conductance–voltage plot (Fig. 6 *A*). Conductance was maximal at +50 mV and the normalized conductance (g/g_{max}) was taken to be equivalent to n_∞^4 such that $n_\infty = \sqrt[4]{g/g_{max}}$. The data are well described by a fourth power Boltzmann function of the form: g/g_{max} $(n_\infty^4) = 1/[1 + \exp[(V_m - V_{1/2})/s]]^4$,

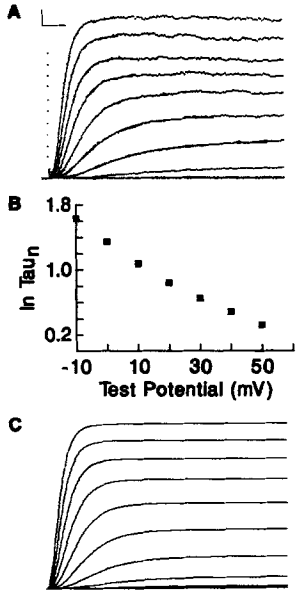

FIGURE 5. Modeling of outward current activation. (*A*) I_{out} waveforms (plotted as points) recorded in a typical atrial cell during the first 40 ms after voltage steps from a HP of −60 mV to potentials between −40 and +50 mV in 10-mV increments are displayed. The activation phases of the currents evoked at −10 to +50 mV are shown fitted (*solid lines*) to fourth power exponentials of the form $I_{out}(t) = I_{max} * [1 - \exp(-t/\tau_n)]^4$ (see text). (*B*) Mean ln τ_n values (n = 56) determined from the fits of I_{out} activation are plotted as a function of test potential. (*C*) Simulated I_{out} waveforms during voltage steps identical to those in *A* (see text). Calibration bars: 400 pA and 4 ms (*A*).

with a half-maximal activation value ($V_{1/2}$) of −32 mV, corresponding to an n_∞ value of 0.5 (Fig. 6 *A*). Lower power Boltzmann functions did not fit the activation data as well as when $n = 4$.

The values of α and β at each voltage were best fitted (Fig. 6, *B* and *C*, solid lines) with continuous functions of voltage of the form:

$$\alpha(s^{-1}) = 10 * \left\{ \frac{(V_m + 17)}{1 - \exp\left[\frac{(-V_m - 17)}{10}\right]} \right\}$$

$$\beta(s^{-1}) = 50 * \exp\left[\frac{(-V_m - 15)}{37}\right]$$

where V_m is the membrane potential. Since these functions adequately describe the data (Fig. 6), they were used in the simulations rather than the individual values for α and β at each voltage. As can be seen in Fig. 5 *C*, the waveforms of the simulated currents evoked during brief depolarizations to −40 to +50 mV from a HP of −60 mV closely resemble I_{out} measured in a typical atrial cell (Fig. 5 *A*).

To account for voltage-independent inactivation without substantial inactivation of closed channels at the resting potential, it has been suggested that inactivation must

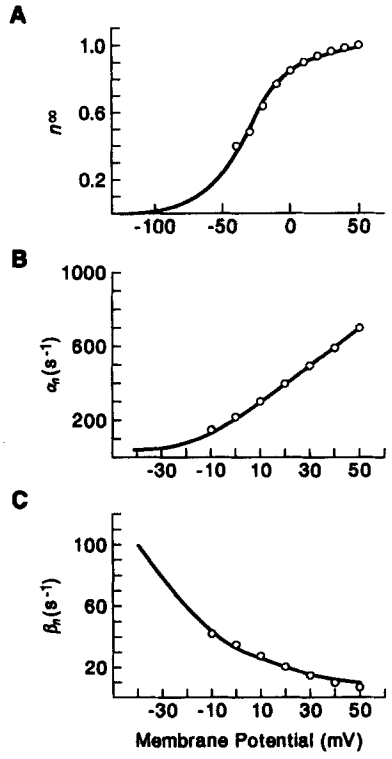

FIGURE 6. Modeling of activation rate constants and steady-state current activation. (*A*) Mean (±SEM) normalized membrane conductances for peak I_{out} (n = 56) during depolarizations to potentials from −40 to +50 mV (HP −60 mV), calculated assuming a reversal potential of −75 mV (see text). Note that no error bars are apparent because the symbols themselves reflect the mean ± SEM. The data points are shown fitted (*solid line*) to a fourth power Boltzmann function with a $V_{1/2}$ of −32 mV corresponding to an n_∞ value of 0.5 (see text). It is important to point out that, in spite of the apparent goodness of the fit, the reliability of low n_∞ values is limited due to the fact that this is a fourth power function. (*B*) The n_∞ values derived from the conductance–voltage plot (in *A*) and the τ_n values derived from analyses of the kinetics of I_{out} activation (Fig. 5 *B*) were used to calculate the voltage-dependent activation rate constants (α) where $\alpha = n_\infty/\tau_n$. The calculated values (plotted as points) are shown fitted (*solid line*) to a continuous Hodgkin-Huxley function of voltage (see text). (*C*) Voltage-dependent deactivation (closing) rate constants (β) were calculated from the same data as in *B*, where $\beta = (1 - n_\infty)/\tau_n$. The calculated values for β (plotted as points) were fitted (*solid line*) to a continuous Hodgkin-Huxley function of voltage (see text).

be coupled to activation (DeCoursey, 1990; Koren et al., 1990; Zagotta and Aldrich, 1990). The rate constants controlling inactivation and recovery from inactivation are voltage independent, and inactivation thereby derives only an "apparent" voltage dependence from the voltage-dependent forward (α) and backward (β) rate constants for activation. This coupled gating model is consistent with the observed voltage-independent inactivation of I_{out} (Fig. 2 *C*) and in all the models tested (see below) the inactivation and recovery rate constants could be adjusted to approximate the time

courses of inactivation at +50 mV and recovery from inactivation at −60 mV observed in atrial cells.

Simulations of the currents evoked during single voltage steps with models incorporating multiple inactivation pathways revealed outward current waveforms that were similar to those observed in the typical atrial cell. However, these models could not account for the experimentally observed complete recovery of I_{Kf} independent of I_{Ks} recovery. Successive depolarizations presented at varying interpulse intervals with these models demonstrated that the complete recovery of I_{Kf} requires the complete recovery of I_{Ks}. In fact, simulations with these and other similar models in which the two current components shared any kinetic state(s) along the gating pathway indicated that complete recovery of the shared state is required for the complete recovery of either component. Recovery from inactivation of the simulated currents could be reconciled with the experimental data only when I_{out} was modeled as two functionally separate currents (I_{Kf} and I_{Ks}) with no shared kinetic states. These results are interpreted as consistent with the interpretation (discussed above) that I_{Kf} and I_{Ks} are functionally independent channel populations.

All subsequent modeling, therefore, was completed with I_{Kf} and I_{Ks} treated as two functionally distinct gating pathways. This required that we determine directly if the voltage dependences of activation of these two current components were indeed identical, as suggested by the data in Fig. 2 and as assumed in the initial modeling (see above). To do this, it was necessary to design voltage-clamp paradigms that would allow the reversal potentials and the kinetics of activation of I_{Kf} and I_{Ks} to be measured independently. This was achieved experimentally by taking advantage of the differing time courses of inactivation and recovery from inactivation of I_{Kf} and I_{Ks}. Specifically, to determine the reversal potential of I_{Ks}, hyperpolarizing test pulses were presented 1 s after the onset of depolarizations to +50 mV (i.e., at a time when I_{Kf} is inactivated and I_{Ks} remains); the resulting tail currents should largely reflect the deactivation of I_{Ks}. To determine the reversal potential of I_{Kf}, it was necessary to use a more complicated voltage-clamp paradigm. In this case, cells were first depolarized to +50 mV for 10 s, followed by a 1-s repolarization to −70 mV (i.e., a time sufficient to allow nearly complete recovery of I_{Kf} but little or no recovery of I_{Ks}). A second depolarization to +50 mV was then presented to evoke I_{Kf}, and the reversal potential of this component was determined from tail currents evoked on hyperpolarizations presented at the peak of the outward current. Linear interpolation of the tail current amplitudes measured 2.5 ms after the onset of the hyperpolarizations provided mean (±SD) reversal potentials for I_{Kf} and I_{Ks} of −76.2 ± 1.6 and −75.8 ± 2.0 mV, respectively. These values are not significantly different from each other or from the average value of −75.5 ± 1.6 mV for the composite current determined previously (Boyle and Nerbonne, 1991). These values are, however, positive to the calculated value of E_K under the recording conditions used (~ −90 mV). Thus, it appears that, although K^+ selective, I_{Kf} and I_{Ks}, like the composite I_{out} channels (Boyle and Nerbonne, 1991), have finite permeabilities to other ions.

A protocol similar to that used to determine the reversal potential of I_{Ks} (above) was employed to examine I_{Ks} activation, except that after the initial depolarization to +50 mV, cells were repolarized to −70 mV for 5 ms (insufficient time for I_{Kf} to recover) and then depolarized to potentials between −40 and +60 mV to activate I_{Ks}. To examine I_{Kf} activation, a protocol similar to that described above was also used,

except that after the 1-s repolarization to −70 mV, cells were depolarized to test potentials of −40 to +60 mV. The kinetics of activation of the evoked currents, which reflect only I_{Kf}, were then analyzed. These experiments confirmed that both I_{Kf} and I_{Ks} activate rapidly on membrane depolarization, and that the kinetics of activation of the two components are indistinguishable from each other and from those of the composite I_{out}. All subsequent modeling was completed, therefore, with I_{Kf} and I_{Ks} treated as two functionally separate currents with identical kinetics and voltage dependences of activation.

Three basic gating models ultimately emerged that could account for the observed activation, inactivation, and recovery data. These are illustrated below and the rate constants for inactivation (κ) and recovery from inactivation (λ) used in the models are provided in the accompanying tables.

$$C_1 \underset{\beta}{\overset{4\alpha}{\rightleftharpoons}} C_2 \underset{2\beta}{\overset{3\alpha}{\rightleftharpoons}} C_3 \underset{3\beta}{\overset{2\alpha}{\rightleftharpoons}} C_4 \underset{4\beta}{\overset{\alpha}{\rightleftharpoons}} O \underset{\lambda}{\overset{\kappa}{\rightleftharpoons}} I \tag{B}$$

	$\kappa(s^{-1})$	$\lambda(s^{-1})$
I_{Kf}	8	1.6
I_{Ks}	0.4	0.08

$$\begin{array}{ccccccc} C_1 & \underset{\beta}{\overset{4\alpha}{\rightleftharpoons}} & C_2 & \underset{2\beta}{\overset{3\alpha}{\rightleftharpoons}} & C_3 & \underset{3\beta}{\overset{2\alpha}{\rightleftharpoons}} & C_4 \underset{4\beta}{\overset{\alpha}{\rightleftharpoons}} O \\ & & \lambda \uparrow\downarrow \kappa & & \lambda \uparrow\downarrow 2\kappa & & \lambda \uparrow\downarrow 3\kappa \quad \lambda \uparrow\downarrow 4\kappa \\ & & I_1 & \underset{\beta}{\overset{3\alpha}{\rightleftharpoons}} & I_2 & \underset{2\beta}{\overset{2\alpha}{\rightleftharpoons}} & I_3 \underset{3\beta}{\overset{\alpha}{\rightleftharpoons}} I_4 \end{array} \tag{C}$$

	$\kappa(s^{-1})$	$\lambda(s^{-1})$
I_{Kf}	2	1.6
I_{Ks}	0.1	0.08

$$\begin{array}{ccccccccc} C_1 & \underset{\beta}{\overset{4\alpha}{\rightleftharpoons}} & C_2 & \underset{2\beta}{\overset{3\alpha}{\rightleftharpoons}} & C_3 & \underset{3\beta}{\overset{2\alpha}{\rightleftharpoons}} & C_4 & \underset{4\beta}{\overset{\alpha}{\rightleftharpoons}} & O \\ & & \lambda \uparrow\downarrow \kappa & & \lambda \uparrow\downarrow 2\kappa & & \lambda \uparrow\downarrow 3\kappa & & \lambda \uparrow\downarrow 4\kappa \\ & & I_1 & \underset{\beta}{\overset{3\alpha}{\rightleftharpoons}} & I_2 & \underset{2\beta}{\overset{2\alpha}{\rightleftharpoons}} & I_3 & \underset{3\beta}{\overset{\alpha}{\rightleftharpoons}} & I_4 \\ & & & & 2\lambda \uparrow\downarrow \kappa & & 2\lambda \uparrow\downarrow 2\kappa & & 2\lambda \uparrow\downarrow 3\kappa \\ & & & & I_5 & \underset{\beta}{\overset{2\alpha}{\rightleftharpoons}} & I_6 & \underset{2\beta}{\overset{\alpha}{\rightleftharpoons}} & I_7 \\ & & & & & & 3\lambda \uparrow\downarrow \kappa & & 3\lambda \uparrow\downarrow 2\kappa \\ & & & & & & I_8 & \underset{\beta}{\overset{\alpha}{\rightleftharpoons}} & I_9 \\ & & & & & & & & 4\lambda \uparrow\downarrow \kappa \\ & & & & & & & & I_{10} \end{array} \tag{D}$$

	$\kappa(s^{-1})$	$\lambda(s^{-1})$
I_{Kf}	2.2	3.9
I_{Ks}	0.11	0.195

Model B is analogous to models of K^+ channel gating proposed by others in which voltage-independent inactivation is coupled to opening of the channel (DeCoursey, 1990; Koren et al., 1990; Zagotta and Aldrich, 1990). Models C and D allow voltage-independent inactivation from closed states by coupling inactivation to activation of the individual subunits. Thus, inactivation does not occur from the deepest closed state (C_1) in models C and D, and voltage-dependent activation develops as the rate of inactivation (κ to 4κ), as well as the number of channels with at least one activated subunit increases along the gating pathway ($C_2 \rightarrow O$). Both models C and D are consistent with recent data showing that the inactivation "gate" of *Shaker* K^+ channels is an NH_2-terminal cytoplasmic domain of the individual subunits that associates with the activated channel in a voltage-independent manner (Hoshi, Zagotta, and Aldrich, 1990). Model D is analogous to one of the models explored by Zagotta and Aldrich (1990) for gating of *Shaker* K^+ channels in which each of four subunits can inactivate independently after activation. Model C is similar except that, in this model, once a single (activated) subunit inactivates, the channel is functionally inactivated and inactivation of other activated subunits cannot occur. This model (C) appears to be more consistent with the observed concentration dependence of NH_2-terminal peptide-induced inactivation of *Shaker* K^+ channels, which suggests that there is only a single inactivation gate binding site (Zagotta, Hoshi, and Aldrich, 1990).

To simulate the whole-cell current (I_{out}) with each of these models (B–D), I_{Kf} and I_{Ks} were modeled as separate currents with identical activation (α) and deactivation (β) rate constants (see above), and the composite whole-cell current, I_{out}, was modeled as 40% I_{Kf} and 60% I_{Ks}. The ratios of λ to κ for both I_{Kf} and I_{Ks} in these simulations were adjusted to produce a steady-state current (I_{ss}) equal to ~20% of the peak I_{out}, as was observed experimentally (see Table I). The inactivation (κ) and recovery (λ) rate constants for I_{Kf} and I_{Ks} shown in the tables with each of the models were chosen so that all three gating models produced similar simulated I_{out} waveforms with activation and inactivation kinetics which also closely approximated those observed in typical atrial cells (Fig. 7 *A*). Because the two current components were modeled as functionally distinct currents with no shared kinetic states along the gating pathway, I_{Kf} and I_{Ks} recover from inactivation independently (Fig. 7 *B*). In addition, using the rate constants presented in the tables accompanying the models, the time courses of recovery from inactivation of the simulated I_{Kf} and I_{Ks} (Fig. 7 *B*) were similar to those observed experimentally (Fig. 4).

Inactivation late in the activation pathway for both I_{Kf} and I_{Ks} was required to account for the similar voltage-dependent activation properties of peak I_{out}, I_{Kf}, and I_{Ks}. Models in which inactivation occurred only from states early (e.g., C_1 to C_3) in the activation pathway predicted a voltage-dependent decrease in the extent of peak I_{out} inactivation at more depolarized test potentials and therefore different voltage-dependent activation properties of peak I_{out} compared with those of I_{Kf} and I_{Ks}, neither of which was observed experimentally (Fig. 2 *D*). Although these findings exclude closed-state inactivation as the only pathway, they do not eliminate the possibility of multiple inactivation pathways that include some closed-state inactivation (such as in Schemes C and D).

Interestingly, as shown in Fig. 7, *C* and *D*, the models make quite different

predictions regarding the time and voltage dependences of inactivation at membrane potentials <0 mV. For example, models B and C predict substantial slowing of inactivation at membrane potentials <0 mV (Fig. 7 *C*). This "apparent" voltage dependence of inactivation rate (in models B and C) results from the marked slowing

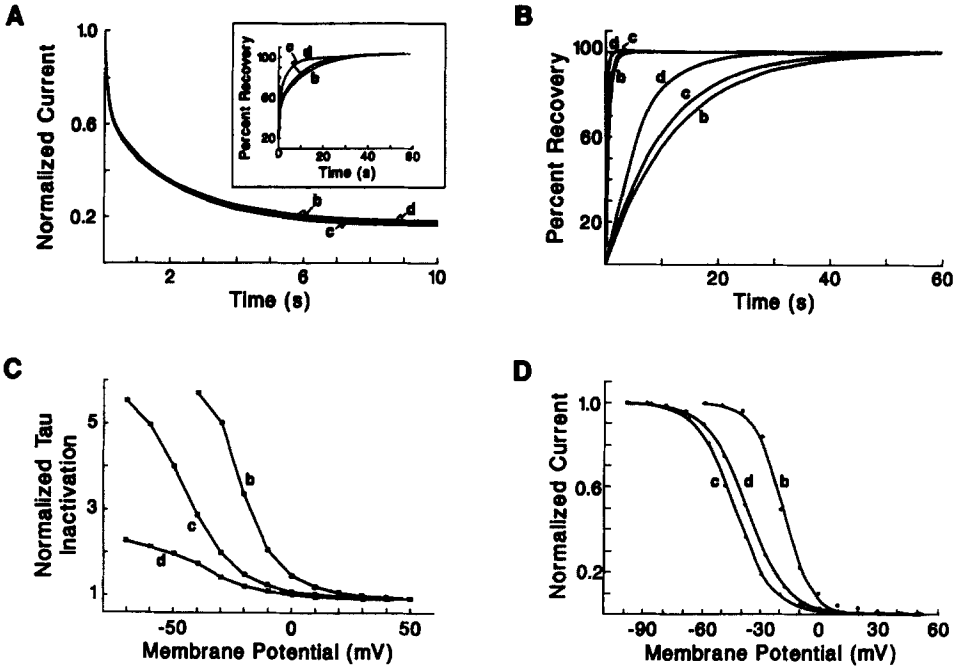

FIGURE 7. Simulations with gating models B, C, and D. For all models, the rates of inactivation of I_{Kf} and I_{Ks} are voltage independent and inactivation is coupled to either channel opening (model B) or subunit activation (models C and D). (*A*) Time course of simulated I_{out} decay during 10-s depolarizations to +50 mV from a HP of −60 mV. Inactivation parameters were adjusted so that the decay phases of the simulated I_{out} were similar for all three models (see text). (*Inset*) Time course of recovery at −60 mV of the simulated peak I_{out} after a 10-s depolarization to +50 mV. (*B*) Time course of recovery at −60 mV of the simulated I_{Kf} and I_{Ks} components of the (simulated) peak I_{out} after 10-s depolarizations to +50 mV. In all three models, I_{Kf} recovers rapidly (left three traces) and I_{Ks} recovers ~20 times more slowly (right three traces). (*C*) Inactivation time constants of the simulated currents plotted as a function of test potential. Time constants were normalized to values obtained for the +50-mV depolarization. (*D*) Voltage dependence of inactivation of the simulated currents. The data (plotted as points) derived from the simulations were fitted (*solid lines*) with single Boltzmann functions; the best fits to the data points yielded $V_{1/2}$ values of −19, −46, and −39 mV for models B, C, and D, respectively.

of current activation. With model D, in contrast, there is much less effect of membrane potential on the apparent rate of inactivation as compared with the predictions with models B and C (Fig. 7 *C*). The results obtained from the simulations of voltage-dependent inactivation with these models are shown fitted in Fig. 7 *D*

to Boltzmann functions (solid lines) of the form:

$$I(V) = 1/[1 + \exp[(V - V_{1/2})/s]] \quad (2)$$

where $I(V)$ is the normalized current as a function of the HP (V), $V_{1/2}$ is the voltage at which 50% of the channels are inactivated, and s is the slope factor. Model B, in which inactivation is coupled to channel opening, predicts a $V_{1/2}$ for inactivation (for I_{Kf} and I_{Ks}) of −19 mV. Models C and D, in which inactivation is coupled to activation of the individual subunits, however, predict $V_{1/2}$ values of −46 and −39 mV, respectively. These predictions of models B–D regarding the time and voltage

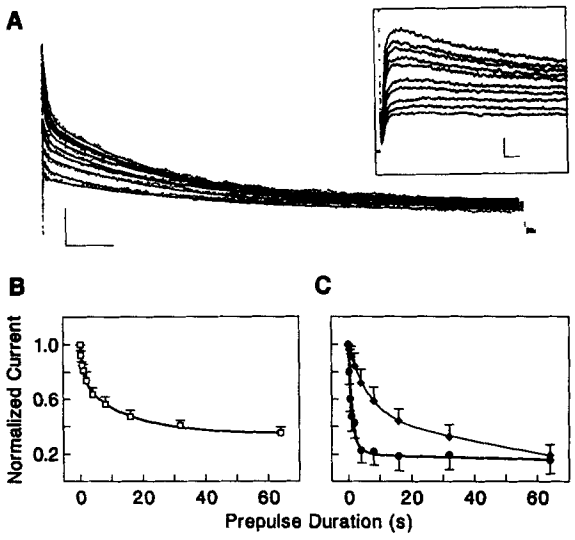

FIGURE 8. The apparent rates of inactivation of peak I_{out}, I_{Kf}, and I_{Ks} are slowed at −30 mV. (*A*) I_{out} waveforms recorded during 10-s depolarizations to +50 mV directly from −90 mV (*top record*) or after prepulses (to −30 mV) of varying durations up to 64 s (*bottom record*). The decay phases of I_{out} are shown fitted to a double exponential function with time constants of 118 ms and 2.8 s; from these fits the amplitudes of I_{Kf} and I_{Ks} were determined (see text). (*Inset*) The first 100 ms of currents recorded during the 10-s depolarizations to +50 mV are shown on an expanded time scale. (*B*) Inactivation of peak I_{out} as a function of prepulse duration. Peak I_{out} amplitudes measured during +50-mV depolarizations preceded by varying duration prepulses were normalized to the peak I_{out} evoked directly from −90 mV, and are plotted as a function of prepulse duration. Mean (±SEM; n = 4) data are shown fitted with a double exponential decay function (*solid line*) with time constants of 980 ms and 13.1 s. (*C*) Normalized I_{Kf} (●) and I_{Ks} (◆) amplitudes determined from the fits of I_{out} decay are plotted as functions of prepulse duration. Mean (±SEM; n = 4) data are shown fitted with single exponential functions (*solid lines*); I_{Kf} and I_{Ks} inactivations were fitted with time constants of 1,060 ms and 11.4 s, respectively. Calibration bars: 500 pA and 1 s (*A*); 400 pA and 10 ms (inset of *A*).

dependences of inactivation of I_{Ks} and I_{Kf} at membrane potentials <0 mV were then tested experimentally in atrial cells in an attempt to distinguish among the models.

Steady-State Inactivation

The time courses of inactivation of peak I_{out}, I_{Kf}, and I_{Ks} at membrane potentials negative to 0 mV were examined by application of varying duration prepulses to −30 mV from a HP −90 mV before the 10-s depolarizations to +50 mV (Fig. 8). The decay of peak I_{out} during depolarization directly from −90 mV was fitted (Eq. 1) and the values for τ_f and τ_s obtained from this fit were then used to fit I_{out} decay during

subsequent depolarizations that were preceded by prepulses; depolarizations were presented at 60-s intervals to allow complete recovery of peak I_{out}. In Fig. 8 *A*, data are shown from one such experiment in which 250-ms to 64-s prepulses to −30 mV were applied. Using the values of τ_f and τ_s derived from the fit of the current evoked directly from −90 mV (Fig. 8 *A*, top trace), the decay phases of I_{out} evoked from each prepulse potential were well described. In these experiments, the first 100 ms of the +50-mV depolarization was recorded at a high sampling frequency (Fig. 8 *A*, *inset*) to allow parallel assessment of the rate of I_{out} activation (see below).

To determine the kinetics of I_{out}, I_{Kf}, and I_{Ks} inactivation at −30 mV, the currents were normalized to their respective maximal values measured during the depolarization with no prepulse. The mean (±SEM; $n = 4$) normalized current amplitudes are plotted as a function of prepulse duration and fitted to exponential decay functions in Fig. 8, *B* and *C*. The time course of peak I_{out} decay was best fitted ($R = 0.99$) by the sum of two exponentials using Eq. 1 (above) with time constants of 980 ms and 13.1 s (Fig. 8 *B*). As shown in Fig. 8 *C*, the inactivation time courses of I_{Kf} and I_{Ks} plotted separately were well described ($R = 0.99$) by single exponentials with similar time constants of 1,060 ms and 11.4 s, respectively. These results indicate that I_{Kf} and I_{Ks} can be distinguished based on their differing inactivation kinetics at membrane potentials <0 mV. In addition, both I_{Kf} and I_{Ks} inactivate approximately five times more slowly at −30 mV than at +50 mV, consistent with the slowing of inactivation predicted by models B and C (Fig. 7 *C*). Although the rates of I_{Ks} and I_{Kf} inactivation at −30 mV were measured indirectly in these experiments, the validity of the conclusions is supported by the finding that the inactivation time constants for I_{Kf} and I_{Ks} derived from the fits were essentially identical to those that described the time course of peak I_{out} inactivation. In addition, as shown in the inset of Fig. 8 *A*, there was no measurable change in activation rate when the current amplitude was decreased by the prepulses. Because the short duration prepulses selectively inactivated I_{Kf}, these data (Fig. 8 *A*, *inset*) illustrate that I_{Ks} activates rapidly on membrane depolarization with kinetics of activation that are indistinguishable from those of I_{out} (see also above). With long duration prepulses, both I_{Kf} and I_{Ks} are completely inactivated, and the residual current (I_{ss}) also activates rapidly, consistent with the assumption noted above that I_{ss} represents the noninactivating portions of I_{Kf} and I_{Ks}.

The voltage dependences of steady-state inactivation of peak I_{out}, I_{Kf}, and I_{Ks} were determined at HPs between −90 and 0 mV (Fig. 9). Cells were held at each HP for 64 s to ensure that steady state was reached before the 10-s depolarizations to +50 mV to evoke the outward currents; a 60-s recovery period at a HP of −90 mV was allowed between each pulse sequence. More hyperpolarized HPs (−100 to −120 mV) did not result in measurable increases in peak I_{out}, I_{Kf}, or I_{Ks}. In these experiments, I_{out} measured during a 10-s depolarization to +50 mV directly from −90 mV was fitted first and the values for τ_f and τ_s obtained from this fit were then used to fit I_{out} decay during subsequent depolarizations from the more depolarized HPs (Fig. 9 *A*). I_{out}, I_{Kf}, and I_{Ks} amplitudes were then normalized to the values obtained for the depolarization directly from −90 mV, and the mean (±SEM, $n = 3$) normalized current amplitudes are plotted a function of HP in Fig. 9, *B* and *C*. The Boltzmann fit to the data for peak I_{out} (Fig. 9 *B*, solid line) yielded values of $V_{1/2} = -44$ mV and $s = 10$ mV ($R = 0.99$). The variations in I_{Kf} and I_{Ks} amplitudes with HP were similar (Fig.

9 *C*) with the best fits yielding $V_{1/2} = -46$ mV and $s = 8$ mV ($R = 0.99$) for I_{Kf}, and $V_{1/2} = -43$ mV and $s = 11$ mV ($R = 0.99$) for I_{Ks}. Both the time- and voltage-dependent inactivation properties of I_{Kf} and I_{Ks} at membrane potentials <0 mV thus appeared strikingly similar to those predicted by model C (Fig. 7 *D*). In particular, model C predicted the slowing of inactivation at membrane potentials <0 mV and a $V_{1/2}$ essentially identical to that observed experimentally (see Discussion).

Pharmacologic Sensitivity of the Currents

The sensitivities of I_{Kf} and I_{Ks} to extracellular 4-AP and TEA were examined during repetitive 10-s depolarizations to +50 mV from a HP of −60 mV delivered at 60-s

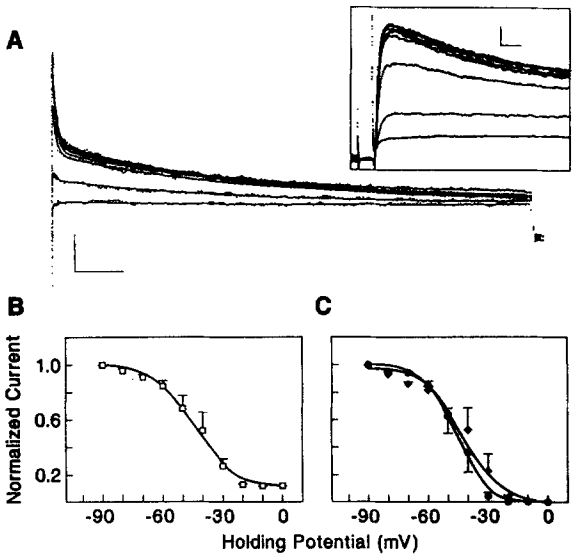

FIGURE 9. Voltage-dependent inactivation of peak I_{out}, I_{Kf}, and I_{Ks}. (*A*) I_{out} (plotted as points) evoked from HPs between −90 mV (*top record*) and −20 mV (*bottom record*) are shown fitted to a double exponential decay function with time constants of 98 ms and 3.7 s (see text). In each case, the cell was held at the HP for 64 s before depolarization to +50 mV to ensure that steady state was achieved. HPs between −50 and −20 mV resulted in progressive decreases in the amplitude of the currents evoked on depolarization to +50 mV. (*Inset*) The first 100 ms of the currents recorded during the 10-s depolarizations to +50 mV are shown on an expanded time scale. (*B*) Mean (±SEM; $n = 3$) normalized peak I_{out} are plotted as a function of HP. Inactivation of peak I_{out} is shown fitted by a single Boltzmann function (*solid line*) with $V_{1/2} = -44$ mV and $s = 10$ mV. (*C*) Mean (±SEM; $n = 3$) normalized I_{Kf} (●) and I_{Ks} (◆) amplitudes determined from fits of I_{out} decay plotted as functions of HP are shown fitted to single Boltzmann functions (*solid lines*) with $V_{1/2}$ values of −46 and −43 mV for I_{Kf} and I_{Ks}, respectively. Calibration bars: 600 pA and 1 s (*A*); 400 pA and 10 ms (inset of *A*).

intervals. The cells were then exposed to 4-AP or TEA continuously for at least 2 min to allow the level of block to stabilize. The extent of I_{Kf} and I_{Ks} attenuation was determined by comparing the amplitudes of the current components derived from the pre- and posttreatment fits of I_{out} decay; the values for τ_f and τ_s determined from the pretreatment fit were used for the posttreatment fits. As shown in Fig. 10, *A* and *B*, puffer applications of 1 and 5 mM 4-AP were accompanied by marked attenuation of peak I_{out}, I_{Kf}, and I_{Ks}. As shown in Table II, the percent block (mean ± SD) by 4-AP appeared to be dose dependent over the concentration range of 1 mM ($n = 3$) to 5 mM ($n = 4$), and the effects of 4-AP on I_{Kf} and I_{Ks} were similar.

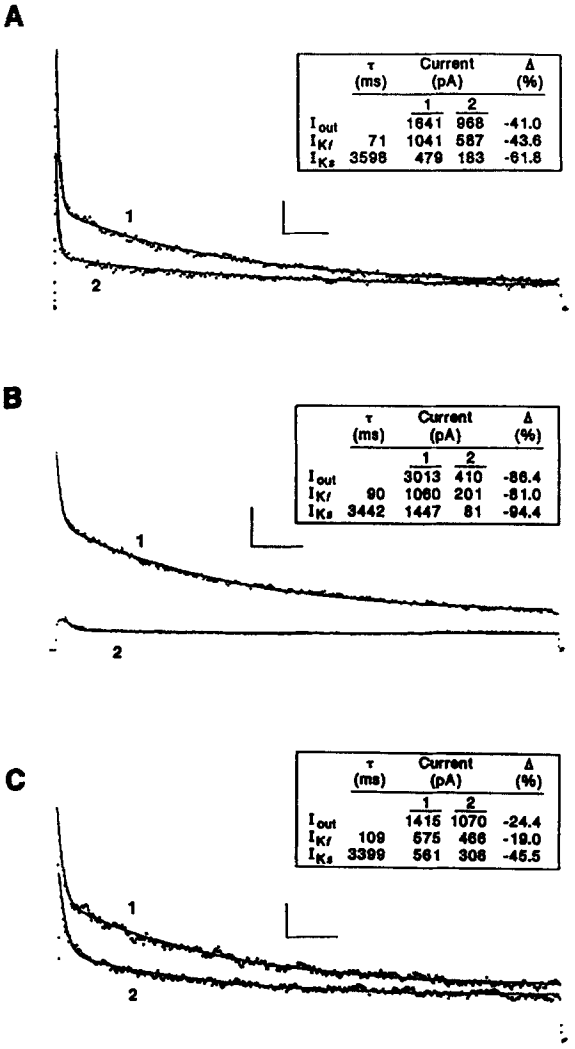

FIGURE 10. Blockade of I_{out}, I_{Kf}, and I_{Ks} by (*A*, *B*) 4-AP and (*C*) TEA. In all three panels, I_{out} evoked during 10-s depolarizing pulses to +50 mV from a HP of −60 mV was recorded before (*1*) and during (*2*) continuous application of 1 mM 4-AP (*A*), 5 mM 4-AP (*B*), or 50 mM TEA (*C*) to the surface of the cell from a puffer pipette (see Methods). The decay phases of I_{out} are plotted as points and the double exponential fits to the decay phases are plotted as solid lines. From these, the amplitudes of I_{Kf}, I_{Ks}, and I_{ss} were calculated (see text). (*Insets*) The magnitudes of peak I_{out}, I_{Kf}, and I_{Ks} determined from the fits are displayed, together with the percent change (Δ) in the currents produced by the drug application, calculated as $[(I_2 - I_1)/I_1] * 100$. Calibration bars: 200 pA and 1 s (*A*, *C*); 500 pA and 1 s (*B*).

TABLE II

Percent Block of Atrial I_{out} by 4-AP and TEA

	5 mM 4-AP (n = 4)	1 mM 4-AP (n = 3)	50 mM TEA (n = 7)
I_{out}	82.6 ± 8.2	47.6 ± 5.3	24.4 ± 11.9*
I_{Kf}	90.7 ± 7.6	66.1 ± 19.5	27.8 ± 17.1*
I_{Ks}	97.7 ± 2.4	76.3 ± 7.8	40.6 ± 17.7*

Mean ± SD.

*P < 0.05 compared with 1 or 5 mM 4-AP.

An example of the effect of 50 mM TEA on the outward currents is shown in Fig. 10 *C*. Qualitatively similar results were obtained in six other atrial cells (Table II). Although there was some cell to cell variability in the response to TEA, when data from many cells ($n = 7$) were averaged, the degrees to which I_{Kf} and I_{Ks} were affected by TEA were not significantly different (Table II). Thus, these experiments reveal that both I_{Kf} and I_{Ks} display similar sensitivities to 4-AP and that both currents are relatively insensitive to externally applied TEA. In addition, we found that the effects of 4-AP and TEA on the noninactivating current (I_{ss}) are essentially identical to those seen on I_{Kf} and I_{Ks} (see Fig. 10), again consistent with the assumption (noted previously) that I_{ss} represents the noninactivating fractions of I_{Kf} and I_{Ks}.

DISCUSSION

The results presented here reveal the presence of two components, I_{Kf} and I_{Ks}, of the total Ca^{2+}-independent, depolarization-activated outward currents (I_{out}) in adult rat atrial myocytes with distinct rates of inactivation and recovery from inactivation. In particular, I_{Kf} inactivates and recovers from inactivation ~20 times more rapidly than I_{Ks}. Although previously we noted that peak I_{out} is stable during repetitive 100-ms depolarizations presented at 5-s intervals (Boyle and Nerbonne, 1991), the experiments here indicate that considerably longer interpulse intervals are needed for complete recovery of peak I_{out} after long depolarizations. These experiments also reveal that the difference in the time courses of recovery of peak I_{out} after brief and long depolarizations is due to the distinct inactivation and recovery kinetics of I_{Kf} and I_{Ks}. During brief steps, only I_{Kf} inactivates to any extent. Recovery of peak I_{out}, then, parallels the recovery of I_{Kf} and is complete within a few seconds. In contrast, I_{Ks} inactivates only during long depolarizations, and the slow recovery of this component results in the long interpulse intervals required for complete recovery of peak I_{out} after long depolarizations.

Interestingly, other than the differences in the kinetics of inactivation and recovery from inactivation, the two components of I_{out} could not be distinguished by other established criteria for separating K^+ currents. This primarily reflects the fact that I_{Kf} and I_{Ks} display indistinguishable voltage dependences and kinetics of activation and similar sensitivities to 4-AP and TEA. Nevertheless, the observation that I_{Kf} recovery from inactivation is independent of I_{Ks} recovery indicates that I_{Kf} and I_{Ks} cannot share any kinetic states and therefore are functionally independent currents. I_{Kf} and I_{Ks} could reflect alternate pathways for gating of a single type of K^+ channel; however, if they do, interconversion between the two gating pathways must be too slow to be evident during the time course of our experiments.

From a physiological standpoint, the rapid activation of I_{Kf} and I_{Ks} suggests that both components contribute to repolarization of the action potential (AP) in adult rat atrial myocytes. In addition, the relatively slow rates of recovery from inactivation, particularly for I_{Ks}, suggest that the amount of steady-state inactivation may vary considerably as a function of stimulation frequency. Thus, accumulation of inactivation of one or both components may occur at the high heart rates observed under normal physiological conditions in the rat. In this regard, the physiological roles of I_{Kf} and I_{Ks} may differ. The relatively rapid inactivation and recovery of I_{Kf} compared

with I_{Ks} suggest that changes in the steady-state availability of this current after a change in heart rate would occur relatively rapidly. In contrast, the slow inactivation and recovery of I_{Ks} suggest that changes in the availability of this current would occur more slowly. Interestingly, accumulated inactivation of 4-AP-sensitive outward currents due to slow recovery has been shown to be the major factor responsible for frequency-dependent changes in AP configuration in other cardiac preparations (Boyett, 1981*a*, *b*; Kukushkin et al., 1983; Mitchell, Powell, Terrar, and Twist, 1984; Escande, Loisance, Planche, and Coraboeuf, 1985; Giles and Van Ginneken, 1985; Giles and Imaizumi, 1988; Litovsky and Antzelevitch, 1988, 1989). Although we have not tested the effect of stimulation frequency directly, the properties of I_{Kf} and I_{Ks} suggest that increasing the heart rate would lead to progressive inactivation of both components, thereby resulting in a higher plateau potential and a longer AP duration. Because AP duration is a primary determinant of the refractory period, progressive lengthening of the AP due to accumulated inactivation would also be expected to increase the refractory period. Thus, the slow recovery of outward currents could serve to protect cells from excessively high stimulation rates that might occur in certain physiological or pathological conditions.

Interestingly, biexponential decay of Ca^{2+}-independent, 4-AP-sensitive outward currents such as observed here for atrial I_{out} has been described previously in other mammalian cardiac preparations. For example, two inactivation time constants reportedly best describe the decay of the 4-AP-sensitive currents in Purkinje fibers from sheep (Kenyon and Gibbons, 1979; Coraboeuf and Carmeliet, 1982), calf (Kenyon and Sutko, 1987), and dog (Nakayama and Fozzard, 1988) heart, in isolated cells from the rabbit atrioventricular node (Nakayama and Irisawa, 1985), atria (Clark, Giles, and Imaizumi, 1988; Giles and Imaizumi, 1988), and ventricles (Hiraoka and Kawano, 1989), and in isolated mouse ventricular myocytes (Benndorf, 1988; Benndorf and Nilius, 1988). Biexponential recovery kinetics have been described for some of these currents (Benndorf and Nilius, 1988; Giles and Imaizumi, 1988; Nakayama and Fozzard, 1988; Hiraoka and Kawano, 1989), although analysis of the independent recovery of the two components has not been reported, and the functional basis for the components has not been determined. Two components of inactivation have been distinguished in the ensemble averages of the currents through a single type (as defined by single channel conductance) of transient K^+ channel in rabbit AV nodal cells with time constants closely resembling those derived from analysis of the decay of the whole-cell current (Nakayama and Irisawa, 1985). Similar results have been reported in rabbit atrial cells (Clark et al., 1988) and for cloned K^+ channels expressed in *Xenopus* oocytes (Koren et al., 1990), suggesting that multiple components of inactivation may arise from a homogenous population of K^+ channels. In contrast, the two components of inactivation of the 4-AP-sensitive transient K^+ current in mouse ventricular cells appear to reflect distinct channel populations (Benndorf, 1988).

In many respects, I_{Kf} in rat atrial cells resembles the transient outward current (I_{to}) in rat ventricular myocytes (Apkon and Nerbonne, 1991). The time and voltage dependences of activation and the pharmacological sensitivities of the two currents are similar. In addition, the inactivation and recovery kinetics of atrial I_{Kf} and ventricular I_{to} are both relatively fast monoexponential processes, albeit ~10 times

faster for ventricular I_{to}. In contrast, the properties of the slowly inactivating rat atrial I_{Ks} and rat ventricular I_K differ markedly. I_K is sensitive to externally applied TEA (Apkon and Nerbonne, 1991) and, in contrast to rat atrial I_{Ks}, rat ventricular I_K is more slowly activating, undergoes voltage-dependent inactivation at more hyperpolarized potentials, and is resistant to 4-AP. Interestingly, the properties of atrial I_{Ks} are remarkably similar to those of several K^+ channels cloned from rat brain and heart cDNA libraries and expressed in *Xenopus* oocytes (Stühmer et al., 1988, 1989; Christie et al., 1989; Grupe et al., 1990; Swanson et al., 1990; Tseng-Crank et al., 1990; Paulmichl et al., 1991; Roberds and Tamkun, 1991).

Although the conclusion here that I_{Kf} and I_{Ks} represent functionally distinct population of channels was reached based purely on kinetic arguments, a variety of potential molecular mechanisms might underlie the distinct kinetic properties of I_{Kf} and I_{Ks}. It is possible, for example, that I_{Kf} and I_{Ks} reflect the expression of two distinct K^+ channel genes. Indeed, several distinct K^+ channel cDNAs have been cloned from rat heart cDNA libraries, including K_v1 (Swanson et al., 1990), RHK1 (Tseng-Crank et al., 1990), RK1 through RK5 (Roberds and Tamkun, 1991), and RAK (Paulmichl et al., 1991). Expression of K_v1 (Swanson et al., 1990) or RAK (Paulmichl et al., 1991) in *Xenopus* oocytes reveals a rapidly activating, slowly inactivating current with kinetic properties similar (but not identical) to I_{Ks}, whereas expression of RHK1 (Tseng-Crank et al., 1990) results in a rapidly activating and inactivating current with electrophysiological and pharmacological properties similar (but not identical) to I_{Kf}. Interestingly, RHK1 differs from K_v1 and RAK mainly in the NH_2-terminal portion of the polypeptide, consistent with the suggestion that the NH_2-terminal sequence is important in determining inactivation kinetics (Kamb, Tseng-Crank, and Tanouye, 1988; Schwarz, Tempel, Papazian, Jan, and Jan, 1988; Timpe, Jan, and Jan, 1988; Hoshi et al., 1990; Zagotta et al., 1990). Thus, I_{Kf} and I_{Ks} may reflect the expression of channels from the same gene family which differ little in terms of primary structure except possibly at the NH_2 terminus. It may also be, however, that coexpression of two alternatively spliced *Shaker* clones (Isacoff, Jan, and Jan, 1990) or two members of the same mammalian K^+ channel gene family (Christie, North, Osborne, Douglass, and Adelman, 1990; Ruppersburg, Schröter, Sakmann, Stocker, Sewing, and Pongs, 1990) results in the expression of K^+ currents with kinetic properties distinct from either gene product expressed alone. Presumably this reflects the formation of heteromultimeric channels. It is possible, therefore, that I_{Kf} and I_{Ks} are heteromultimeric channels that differ only with respect to subunit composition. I_{Kf} and I_{Ks} could also represent different posttranslational modifications of a single type of K^+ channel. Recently, β-adrenergic agonists have been shown to alter the inactivation kinetics of the transient K^+ current in canine ventricular myocytes, presumably due to channel phosphorylation (Nakayama and Fozzard, 1988). Thus, I_{Kf} and I_{Ks} could correspond to distinct gating modes of a homogenous channel population that are modulated by the degree of channel phosphorylation. Certainly, other posttranslational modifications are also possible.

The initial purpose of modeling the atrial K^+ currents was to provide insight into the kinds of kinetic models that could account for the observed kinetics of inactivation and recovery from inactivation. To this end, the modeling provided a direct means of testing the hypothesis that complete recovery of I_{Kf} independent of I_{Ks}

recovery cannot occur if I_{Kf} and I_{Ks} share *any* states in the gating pathway. In addition, a model in which voltage-independent inactivation was coupled to activation of individual subunits produced simulated currents with time- and voltage-dependent properties remarkably similar to those of I_{Kf} and I_{Ks}, as well as those of the composite whole-cell current, I_{out}. This contrasted with the open channel-coupled model, which could account for many of the properties of I_{Kf} and I_{Ks} but predicted a much more depolarized $V_{1/2}$ for inactivation than was observed experimentally. Interestingly, it was possible to apply basic concepts regarding the structure and function of K^+ channels and to construct a gating model for I_{Ks} and I_{Kf} from the whole-cell data that behaves in a manner analogous to the native currents. This strongly suggests that the model reflects features of the gating mechanism of single (I_{Kf} and I_{Ks}) channels. In particular, the subunit activation–coupled model provides for the voltage-independent inactivation observed at depolarized membrane potentials, which has also been observed for a variety of similar K^+ currents (Kenyon and Gibbons, 1979; Giles and Van Ginneken, 1985; Benndorf and Nilius, 1988; Clark et al., 1988; Hiraoka and Kawano, 1989; DeCoursey, 1990; Koren et al., 1990; Zagotta and Aldrich, 1990). This gating mechanism also allows for inactivation of closed channels which was suggested by the hyperpolarized $V_{1/2}$ for inactivation. Zagotta and Aldrich (1990) demonstrated that the rate of inactivation of *Shaker* A-type K^+ channels in *Drosophila* is voltage independent, but also concluded that some closed-state inactivation of those channels must occur to account for the voltage-dependent increase in the number of blank single channel records at less depolarized potentials. Although they found that the subunit activation–coupled model, among other things, predicted too much inactivation at hyperpolarized potentials, we did not find this to be the case for rat atrial I_{Kf} and I_{Ks}. The subunit activation–coupled model predicted $V_{1/2}$ values very similar to those determined experimentally. This model also predicted that the number of channels available to open is not substantially affected over the range of typical resting membrane potentials observed in atrial myocytes (−60 to −90 mV), and this was confirmed experimentally. Thus, we conclude that the subunit activation–coupled model provides a simple model of channel gating that can account for the behavior of the macroscopic depolarization-activated K^+ currents in adult rat atrial myocytes.

We thank Dr. C. J. Lingle and Dr. J. H. Steinbach for many helpful discussions and comments throughout the course of this work and for their careful and critical reading of earlier versions of this manuscript.

We also acknowledge the financial support provided by The National Office of the American Heart Association (Established Investigator Award to J. M. Nerbonne) and the National Institutes of Health (grant HL-34161 to J. M. Nerbonne).

Original version received 13 March 1991 and accepted version received 14 September 1992.

REFERENCES

Apkon, M., and J. M. Nerbonne. 1991. Characterization of two distinct depolarization activated K^+ currents in adult rat ventricular myocytes. *Journal of General Physiology.* 97:973–1011.

Benndorf, K. 1988. Three types of single K channels contribute to the transient outward current in myocardial mouse cells. *Biomedica Biochimica Acta.* 47:401–416.

Benndorf, K., and B. Nilius. 1988. Properties of an early outward current in single cells of the mouse ventricle. *General Physiology and Biophysics.* 7:449–466.

Boyett, M. R. 1981*a*. A study of the effect of the rate of stimulation on the transient outward current in sheep cardiac Purkinje fibers. *Journal of Physiology.* 319:1–22.

Boyett, M. R. 1981*b*. Effect of rate-dependent changes in the transient outward current on the action potential in sheep Purkinje fibers. *Journal of Physiology.* 319:23–41.

Boyle, W. B., and J. M. Nerbonne. 1991. A novel type of depolarization-activated K^+ current in isolated adult rat atrial myocytes. *American Journal of Physiology.* 260:H1236–H1247.

Carmeliet, E., G. Biermans, G. Callawaert, and J. Vereecke. 1987. Potassium current in cardiac cells. *Experientia.* 43:1175–1184.

Christie, M. J., J. P. Adelman, J. Douglass, and R. A. North. 1989. Expression of a cloned rat brain potassium channel in *Xenopus* oocytes. *Science.* 244:221–224.

Christie, M. J., R. A. North, P. B. Osborne, J. Douglass, and J. P. Adelman. 1990. Heteropolymeric potassium channels expressed in *Xenopus* oocytes from cloned subunits. *Neuron.* 2:405–411.

Clark, R. B., W. R. Giles, and Y. Imaizumi. 1988. Properties of the transient outward current in rabbit atrial cells. *Journal of Physiology.* 405:147–168.

Cohen, I. S., N. B. Datyner, G. A. Gintant, and R. P. Kline. 1986. Time-dependent outward currents in the heart. *In* The Heart and Cardiovascular System. H. A. Fozzard, R. B. Jennings, E. Haber, A. M. Katz, and H. E. Morgan. Raven Press, New York. 637–670.

Coraboeuf, E., and E. Carmeliet. 1982. Existence of two transient outward currents in sheep cardiac Purkinje fibers. *Pflügers Archiv.* 392:352–359.

DeCoursey, T. E. 1990. State-dependent inactivation of K^+ currents in rat type II alveolar epithelial cells. *Journal of General Physiology.* 95:617–646.

Escande, D., A. Coulombe, J.-F. Faivre, E. Deroubaix, and E. Coraboeuf. 1987. Two types of transient outward currents in adult human atrial cells. *American Journal of Physiology.* 252:H142–H148.

Escande, D., D. Loisance, C. Planche, and E. Coraboeuf. 1985. Age-related changes of action potential plateau shape in isolated human atrial fibers. *American Journal of Physiology.* 249:H843–H850.

Giles, W. R., and Y. Imaizumi. 1988. Comparison of potassium currents in rabbit atrial and ventricular cells. *Journal of Physiology.* 405:123–145.

Giles, W. R., and A. C. G. Van Ginneken. 1985. A transient outward current in isolated cells from the crista terminalis of rabbit heart. *Journal of Physiology.* 368:243–264.

Grupe, A., K. H. Schroter, J. P. Ruppersberg, M. Stocker, T. Drewes, S. Beckh, and O. Pongs. 1990. Cloning and expression of a human voltage-gated potassium channel: a novel member of the RCK potassium channel family. *EMBO Journal.* 9:1749–1756.

Hamill, O. P., A. Marty, E. Neher, B. Sakmann, and F. J. Sigworth. 1981. Improved patch-clamp techniques for high-resolution current recording from cells and cell-free membrane patches. *Pflügers Archiv.* 391:85–100.

Hiraoka, M., and S. Kawano. 1989. Calcium-sensitive and insensitive transient outward current in rabbit ventricular myocytes. *Journal of Physiology.* 410:187–212.

Hodgkin, A. L., and A. F. Huxley. 1952. A quantitative description of membrane current and its application to conduction and excitation in nerve. *Journal of Physiology.* 117:500–544.

Hoshi, T., W. N. Zagotta, and R. W. Aldrich. 1990. Biophysical and molecular mechanisms of *Shaker* potassium channel inactivation. *Science.* 250:533–538.

Hume, J. R., and A. Uehara. 1985. Ionic basis of the different action potential configurations of single guinea-pig atrial and ventricular myocytes. *Journal of Physiology.* 368:525–544.

Isacoff, E. Y., Y. N. Jan, and L. Y. Jan. 1990. Evidence for the formation of heteromultimeric potassium channels in *Xenopus* oocytes. *Nature.* 345:530–534.

Kamb, A., J. Tseng-Crank, and M. A. Tanouye. 1988. Multiple products of the *Drosophila Shaker* gene may contribute to potassium channel diversity. *Neuron.* 1:421–430.

Kenyon, J. L., and W. R. Gibbons. 1979. 4-Aminopyridine and the early outward current of sheep cardiac Purkinje fibers. *Journal of General Physiology.* 73:139–157.

Kenyon, J. L., and J. L. Sutko. 1987. Calcium- and voltage-activated plateau currents of cardiac Purkinje fibers. *Journal of General Physiology.* 89:921–958.

Koren, G., E. R. Liman, D. E. Logothetis, B. Nadal-Ginard, and P. Hess. 1990. Gating mechanism of a cloned potassium channel expressed in frog oocytes and mammalian cells. *Neuron.* 2:39–51.

Kukushkin, N. I., R. Z. Gainullin, and E. A. Sosunov. 1983. Transient outward current and rate dependence of action potential duration in rabbit cardiac ventricular muscle. *Pflügers Archiv.* 399:87–92.

Litovsky, S. H., and C. Antzelevitch. 1988. Transient outward current prominent in canine ventricular epicardium but not endocardium. *Circulation Research.* 62:116–126.

Litovsky, S. H., and C. Antzelevitch. 1989. Rate dependence of action potential duration and refractoriness in canine ventricular endocardium differs from that of epicardium: role of the transient outward current. *Journal of the American College of Cardiology.* 14:1053–1066.

McDonald, T. F., and W. Trautwein. 1978. The potassium current underlying delayed rectification in cat ventricular muscle. *Journal of Physiology.* 274:217–246.

Mitchell, M. R., T. Powell, D. A. Terrar, and V. W. Twist. 1984. Strontium, nifedipine and 4-aminopyridine modify the time course of the action potential in cells from rat ventricular muscle. *British Journal of Pharmacology.* 81:551–556.

Nakayama, T., and H. A. Fozzard. 1988. Adrenergic modulation of the transient outward current in isolated canine Purkinje cells. *Circulation Research.* 62:162–172.

Nakayama, T., and H. Irisawa. 1985. Transient outward current carried by potassium and sodium in quiescent atrioventricular node cells of rabbits. *Circulation Research.* 57:64–73.

Paulmichl, M., P. Nasmith, R. Hellmiss, K. Reed, W. A. Boyle, J. M. Nerbonne, E. G. Peralta, and D. E. Clapham. 1991. Cloning and expression of a rat cardiac delayed rectifier potassium channel. *Proceedings of the National Academy of Sciences, USA.* 88:7892–7895.

Powell, T., and V. W. Twist. 1976. A rapid technique for the isolation and purification of adult cardiac muscle cells having respiratory control and a tolerance to calcium. *Biochemical and Biophysical Research Communications.* 72:327–333.

Reuter, H. 1984. Ion channels in cardiac cell membranes. *Annual Review of Physiology.* 46:473–484.

Roberds, S. L., and M. M. Tamkun. 1991. Cloning and tissue specific expression of five voltage-gated potassium channel cDNAs expressed in rat heart. *Proceedings of the National Academy of Sciences, USA.* 88:1798–1802.

Ruppersberg, J. P., K. H. Schröter, B. Sakmann, M. Stocker, S. Sewing, and O. Pongs. 1990. Heteromultimeric channels formed by rat brain potassium-channel proteins. *Nature.* 345:535–537.

Schwarz, T. L., B. L. Tempel, D. M. Papazian, Y. N. Jan, and L. Y. Jan. 1988. Multiple potassium-channel components are produced by alternative splicing at the *Shaker* locus in *Drosophila. Nature.* 331:137–142.

Stühmer, W., J. Ruppersberg, K. Schröter, B. Sakmann, M. Stocker, K. Giese, A. Baumann, and O. Pongs. 1989. Molecular basis of functional diversity of voltage-gated K^+ channels in mammalian brain. *EMBO Journal.* 8:3235–3244.

Stühmer, W., M. Stocker, B. Sakmann, P. Seeburg, A. Baumann, A. Grupe, and O. Pongs. 1988. Potassium channels expressed from rat brain cDNA have delayed rectifier properties. *FEBS Letters.* 242:199–206.

Swanson, R., J. Marshall, J. S. Smith, J. B. Williams, M. B. Boyle, K. Folander, C. J. Luneau, J. Antanavage, C. Oliva, S. A. Buhrow, C. Bennett, R. B. Stein, and L. K. Kaczmarek. 1990. Cloning

and expression of cDNA and genomic clones encoding three delayed rectifier potassium channels in rat brain. *Neuron.* 4:929–939.

Timpe, L. C., Y. N. Jan, and L. Y. Jan. 1988. Four cDNA clones from the *Shaker* locus of *Drosophila* induce kinetically distinct A-type potassium currents in *Xenopus* oocytes. *Neuron.* 1:659–667.

Tseng, G.-N., R. B. Robinson, and B. F. Hoffman. 1987. Passive properties and membrane currents of canine ventricular myocytes. *Journal of General Physiology.* 90:671–701.

Tseng-Crank, J. C. L., G.-N. Tseng, A. Schwartz, and M. A. Tanouye. 1990. Molecular cloning and functional expression of a potassium channel cDNA isolated from a rat cardiac library. *FEBS Letters.* 268:63–68.

Wittenberg, B. A., and T. F. Robinson. 1981. Oxygen requirements, morphology, cell coat and membrane permeability of calcium tolerant myocytes from hearts of adult rats. *Cell and Tissue Research.* 216:231–251.

Zagotta, W. N., and R. W. Aldrich. 1990. Voltage-dependent gating of *Shaker* A-type potassium channels in *Drosophila* muscle. *Journal of General Physiology.* 95:29–60.

Zagotta, W. N., T. Hoshi, and R. W. Aldrich. 1990. Restoration of inactivation in mutants of *Shaker* potassium channels by a peptide derived from *ShB*. *Science.* 250:568–571.